Highly-Ordered Growth of Solution-Processable ZnO for Thin Film Transistors

Darragh Buckley[1], David McNulty[1], Vitaly Zubialevich[2], Peter Parbrook[2,3], and Colm O'Dwyer[1,2]

[1] *Department of Chemistry, University College Cork, Cork T12 YN60, Ireland*
[2] *Tyndall National Institute, Lee Maltings, Cork T12 R5CP, Ireland*
[3] *Department of Electrical & Electronic Engineering, University College Cork, Cork T12 YN60, Ireland*

Abstract

We demonstrate that crystalline, epitaxial-like and highly ordered ZnO thin films and quasi-superlattice structures can be achieved from a precursor liquid at relatively low temperature via spin-coating. The synthesised films are smooth, stoichiometric ZnO with controllable thickness. An iterative layer-by-layer coating schematic is employed to demonstrate the effects of film thickness on structure, morphology as well as the surface and internal defects. Characterisation of the crystallinity, morphology, O-vacancy formation, stoichiometry, surface roughness and thickness variation was determined through X-ray diffraction, scanning and transmission electron and atomic force microscopy, X-ray photoelectron and photoluminescence spectroscopy. We demonstrate that iterative spin-coating of deposited ZnO films results in a transition in crystal texture with increasing thickness (number of layers) from the $[10\bar{1}0]$ m-plane to the $[0002]$ c-plane. The films attain a c-axis preferential orientation, with no other crystalline peaks present. Results show that the film's surface morphology was very smooth, with average rms roughness <0.15 nm. Examination of these films also shows the consistency of the surface composition and defect level while highlighting the effect of temperature and cumulative annealing condition on the internal defect concentration.

Introduction

Thin-film transistors (TFTs) are the fundamental building blocks for macroelectronics.(1) They are included in a variety of applications but have their largest application in display technology.(2)-(3) Currently, high field-effect mobility TFTs can be manufactured from low hydrogenated amorphous Si (a-Si:H)(3) however these require vacuum-deposition processes and high fabrication costs. TFTs fabricated from organic semiconductor materials display low field-effect mobilities in comparison to the silicon alternatives but offer a more versatile and less expensive range of materials.

Metal oxide TFTs have a greater performance and stability in TFTs than amorphous silicon devices and are more applicable to transparent, flexible displays which are the foundation of next generation, interactive displays.(4)(5) From the metal oxides, zinc oxide (ZnO)-based materials have attracted increasing attention for use in flexible displays because of their higher mobility and lower processing temperature than conventional hydrogenated amorphous Si (a-Si:H) TFTs.(6, 7) Zinc oxide is an material of interest in the area of optoelectronics due to its wide band gap (E_g ~ 3.3 eV at 300 K)(8), large exciton binding energy (~66 meV) and especially for the variety of methods by which it can be processed(9). Moreover, ZnO is inexpensive, abundant and readily able to alloy with other metals in the oxide form(10-12) and has a lattice that can facilitate interstitial doping.(7) This gives ZnO a key role

in the area of optoelectronics, metal oxide thin films and thin film transistor (TFT) technologies.(13)

As well as their improved characteristics to a-Si:H, metal oxides are investigated for their ability to be fabricated from solution based processes. Solution processes have a number of advantages over high-vacuum and photolithographic methods(14-17); they allow for large-scale, homogenous fabrication at low cost and offers a high degree of compositional control.(18, 19) It is crucial that high crystal quality epitaxial-like thin films can be formed from solution processing to compete with physical deposition methods.

We demonstrate that crystalline, epitaxial-like and highly ordered ZnO thin films can be achieved from a precursor liquid at relatively low temperature via spin-coating. The synthesised films are smooth, stoichiometric ZnO. An iterative layer-by-layer coating schematic is employed to demonstrate the effects of creating a multi-layered thin film on structure, morphology as well as the surface and internal defects. Characterisation of the crystallinity, morphology, O-vacancy formation, stoichiometry and surface roughness was determined through X-ray diffraction, scanning and transmission electron and atomic force microscopy, X-ray photoelectron and photoluminescence spectroscopy.

Experimental

Zinc oxide thin films were synthesised from zinc acetate dihydrate [$Zn(CH_3COO)_2.2H_2O$]. The acetate powder was dissolved in 2-methoxyethanol [$CH_3OCH_2CH_2OH$] to make a 0.75 M solution. An equimolar solution of monoethanolamine (MEA) was added to the zinc precursor as a stabilising agent. All chemicals were purchased from Sigma Aldrich. The precursor was heated at 60 ^oC for 2 h and stirred until a clear, colourless solution is obtained. For comparative analysis, films were also produced from a precursor liquid made by dissolving zinc oxide [ZnO] powder in 28% ammonium hydroxide [NH_4OH] to achieve concentrations between 0.01M and 0.1 M. Controllably thin and smooth films were prepared by a spin-coating technique. Using a SCS G3 desktop spin coater, ZnO precursor solution was added dropwise to cover substrates and were spun at 3000 rpm for 30 s, including a 5 s ramp time.

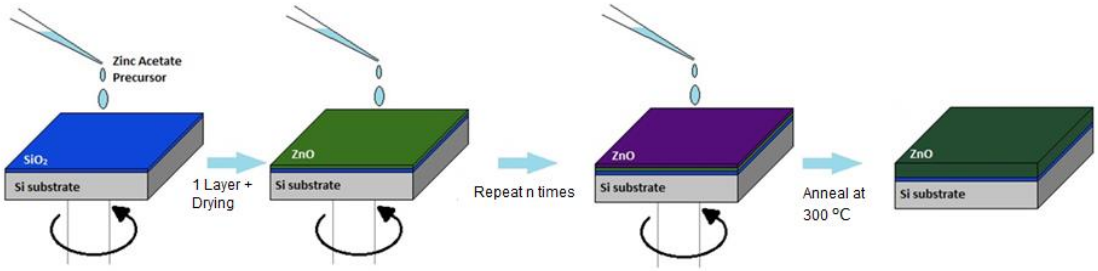

Figure 1. Schematic for the spin coating deposition of ZnO thin films from a liquid precursor.

Thin films were deposited on doped p-type silicon substrates that were covered with a 300 nm thick layer of thermally grown SiO_2. Substrates for spin coated samples were cut into square coupons of nominal dimension 1 cm × 1 cm to ensure even coverage as the samples are rotated about a perpendicular symmetric axis. An acetone, IPA and DI water wash combined with sonication was used to ensure that the surface of the wafers were clean of surface contaminants prior to thin film deposition. A UV-Ozone treatment was performed for 30 mins using a Novascan UV ozone system to further remove any organic contaminants from the surface. After a layer of precursor was spin coated, samples were dried in an open-air

convection oven at temperatures between 250 - 270 ^{o}C for 5 min. Another layer of liquid precursor was then spun onto the surface followed by more oven-drying. This process was then repeated a number of times to acquire the desired number of deposited layers and the samples were subsequently annealed at 300 ^{o}C for 1 hr as a final heat treatment.

Surface morphology of prepared thin films was investigated using Atomic Force Microscopy (AFM) using a Park XE-100 system in non-contact mode with model SSS_NCHR enhanced resolution high aspect ratio tips. The XY and Z resolutions of the AFM stepper motor drives are ~ 2 nm and ~0.05 nm respectively. From AFM data, the root mean square (rms) roughness of the ZnO film surfaces were determined for single- and multi-layer samples.

Transmission electron microscopy (TEM) was conducted on lamellar cross-section of the ZnO thin films on SiO_2/Si. Cross-sectioning of the Si electrodes was carried out with an FEI Helios Nanolab Dual Beam FIB System. Cross-sectional TEM sample preparation was performed on slices using a standard FIB lift-out technique. TEM analysis and electron diffraction was conducted using a JEOL JEM-2100 TEM operating at 200 kV. X-ray diffraction (XRD) was used to characterise the crystallographic structure of the single and multi-layer ZnO films after spin coating deposition. XRD analysis of ZnO films was performed using a Philips X'Pert PW3719 diffractometer using Cu Kα radiation (40 kV and 35 mA) scanned between 10 - 80° (2θ).

The chemical bonding state of the top surface and effective conductivity type were determined by X-ray photoelectron spectroscopy, using a Kratos Axis 165 equipped with a monochromatic Al source (Kα = 1486.58 eV) with a spot size of 1 mm. The source power was 150 W, the take-off angle was set normal to the sample surface, the construction and peak fittings in the narrow region core-level spectra were performed using a Shirley type background. Adventitious carbon was used for the charge reference (C 1s) for each measurement. Photoluminescence (PL) spectroscopy was used to probe the electronic structure of the spin coated ZnO thin films. Band-edge and sub-band PL emission was carried out at room temperature using a 325 nm He–Cd laser excitation source with power density of 2 W/cm^2. PL spectra were recorded using a Horiba iHR320 spectrometer equipped with a thermoelectrically cooled Synapse CCD matrix.

Results and discussion

FIB-thinned lamella of deposited ZnO thin films were examined via TEM to determine the internal structure and to investigate if an iterative spin-coating deposition scheme results in a continuous film or periodic lattice formation. The TEM analysis shown in Fig. 2 shows the cross-sectional structure of a single-layer ZnO thin film and a multi-layer quasi-superlattice (QSL) consisting of 20 individually spin-coated layers. The first deposited layer is shown to uniform in thickness across the SiO_2 substrate. Figure 2(b) displays the layered structure of the multi-layered QSL. Subsequent deposition of material does not interfere with the uniformity of this initial layer. In this periodic structure, each deposition results in a bilayer comprising a dense ZnO material atop a granular sublayer. The drying step (5 min at 260 ^{o}C) between spin-coats results in the formation of the denser capping layer on the upper surface of each deposition, while the sub-layer beneath appears more granular and porous in TEM analysis. This bilayer structure is credited with the epitaxial-like growth of these thin films on amorphous substrates. The resulting QSL or single-layer thin film is crystallised during the final annealing treatment (1 hr at 300 ^{o}C).

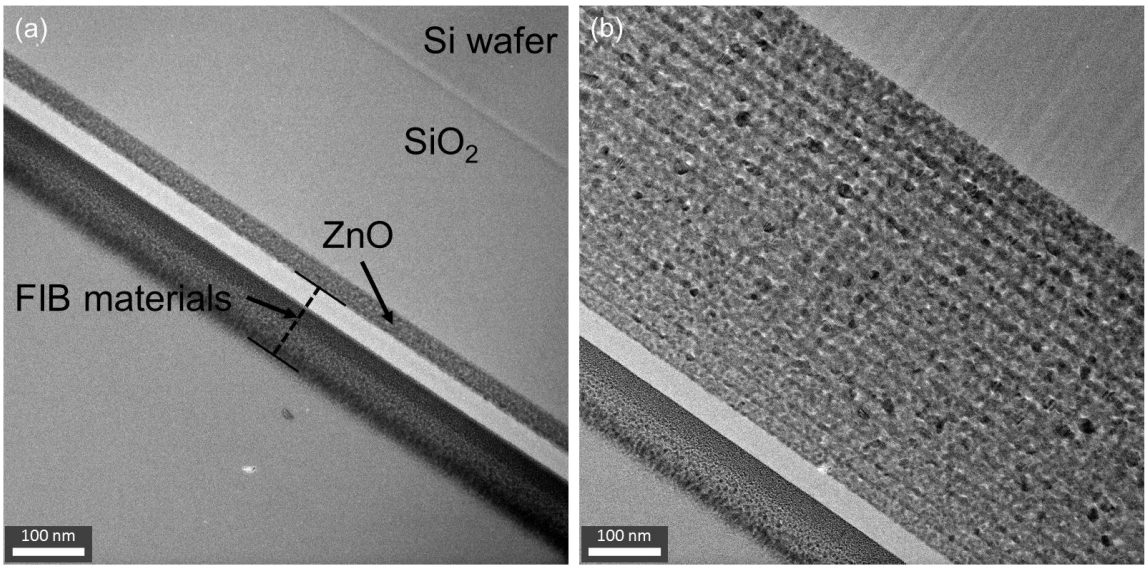

Figure 2. TEM cross-sectional images of (a) 1 layer and (b) 20 layer ZnO thin films grown on SiO_2/Si substrates. The FIB processing materials comprise carbon and Pt straps.

The X-ray diffraction patterns of the 1 and 20 layer thin films shown in Fig. 3 show only two major reflections. These reflections correspond to the m- and c-planes of the ZnO crystal structure. The single layer ZnO film shows only one reflection, implying growth in the [$10\bar{1}0$] direction only. No other [*hkil*] reflections corresponding to wurtzite structure ZnO are present.

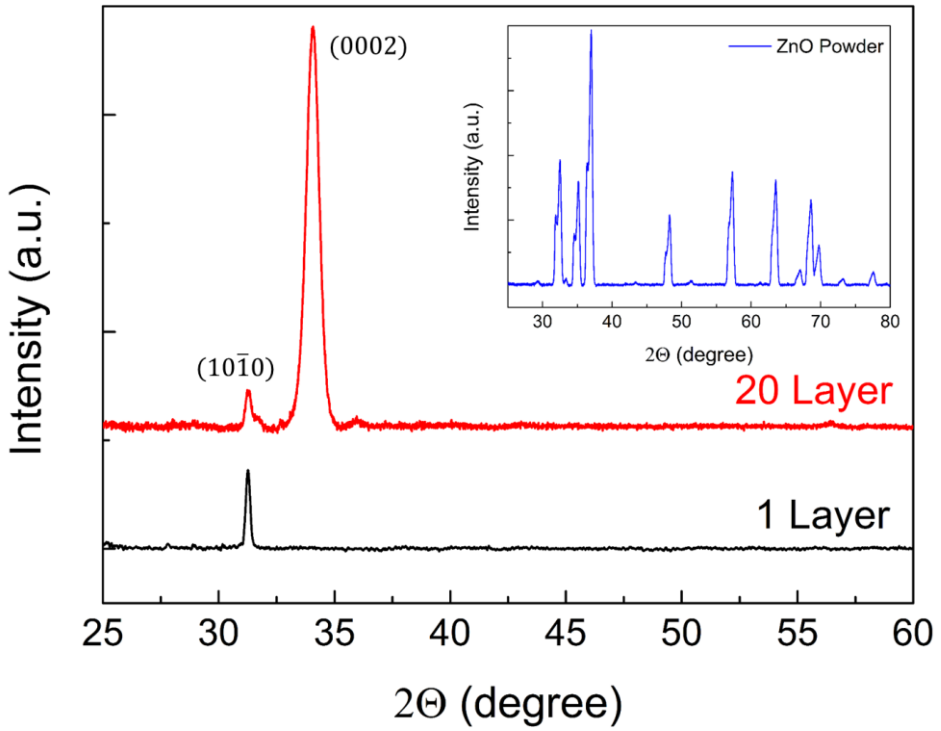

Figure 3. X-ray diffraction patterns for 1 and 20 layer ZnO thin films. Inset is the diffraction pattern for pure ZnO powder.

There is a distinct change in the texture of the crystal growth habit during the sequential process of spin coating additional precursor material and the associated heat treatments. The 20 layer QSL displays a growth preference to the [0002] c-plane direction which is due to the

dense capping layer induced by the drying treatments after each spin-coat. The partially porous layer between these iterative capping layers corresponds to the m-plane reflections still present in the multi-layered film's diffraction pattern. The absence of the other reflections seen in the polycrystalline ZnO pattern acquired from a heated drop-cast powder (inset, Fig. 3) confirms an epitaxial-like growth of spin coated films on an amorphous substrate. This suggests that the initial, dried layer of ZnO on the SiO_2 forms a template for the directed growth of multi-layer or QSL films; subsequent growth however, and cumulative annealing converts the crystal texture to predominantly c-plane orientation.

Cationic and anionic lattice vacancies are an important constituent of semiconducting oxide layers, and primarily influence the unintentional conductivity type (n- or p-type) of the oxide. Oxygen defects are believed to act as electron donors. Oxygen vacancies in the lattice and hydroxyl groups bound to the surface influence the bulk electronic structure and the electronic nature of the surface or interface to metal contacts.(20) Defects such as these can act as trap sites or donors for charge carriers in the film and are therefore an important factors in the charge carrier mobility.

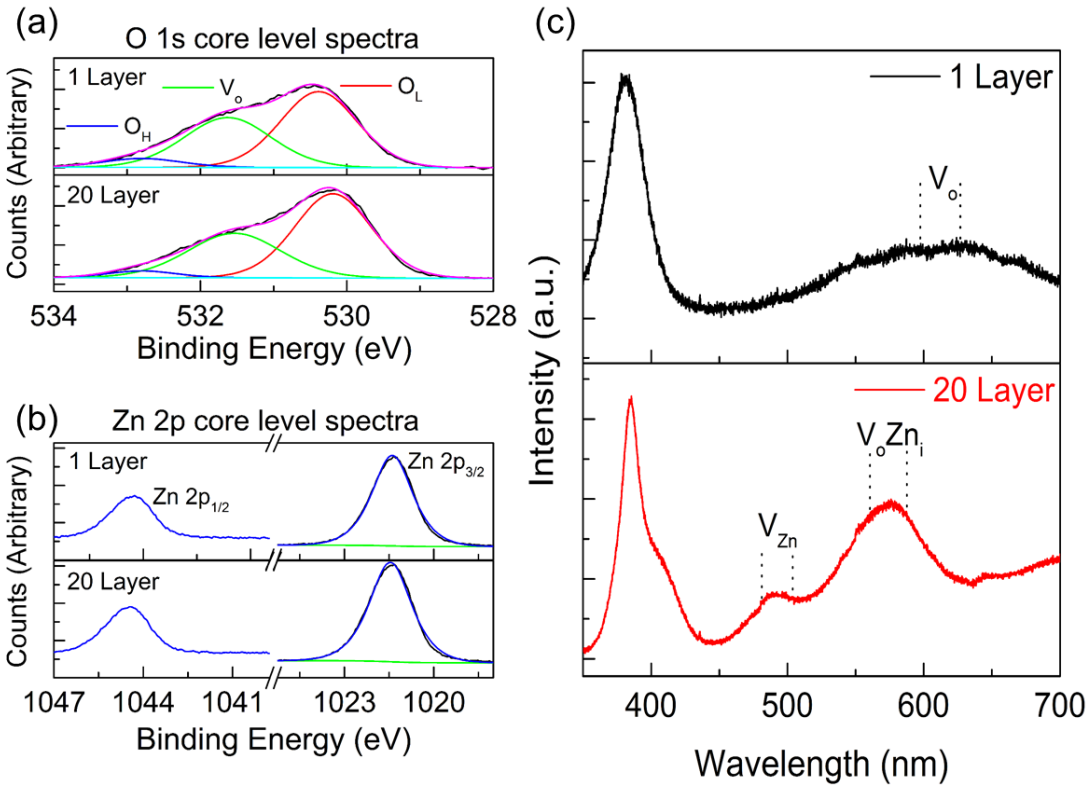

Figure 4. (a) O 1s core level spectra for 1 and 20 layer ZnO thin films. (b) Zn 2p core level spectra. (c) Photoluminescence spectra for 1 and 20 layer ZnO samples.

The O 1s core level spectra, shown in Fig. 4(a), for the single and multilayer samples are asymmetric and comprised of 3 convoluted photoemission peaks. The peaks are centered at ~533 eV, ~531.5 eV and ~530 eV. The lowest energy peak, O_L, at 530 eV is assigned to the O^{2-} ions in the Zn-O lattice bonds and the middle peak, V_O, close to 531.5 eV is associated with O^{2-} ions near oxygen vacant regions.(21) Finally, the highest binding energy peak, O_H, is associated with chemisorbed oxygen in the form of hydroxyl groups.(22) Figure 4(b) shows the Zn 2p spin-orbit doublet core level spectra from XPS measurements. The peak at binding energy of ~1022 eV is assigned to the $2p_{3/2}$, with ~1045 eV assigned to the $2p_{1/2}$ peak. The $2p_{3/2}$

photoemission is nearly symmetric and, as well as the ~23 eV binding energy separation between the doublet peaks, can be assigned to the Zn^{2+} in the formation of ZnO.(23)

As a result of the surface sensitivity of XPS measurements, the consistency of the binding energy and relative intensities of the Zn 2p and O 1s peaks demonstrate that the single and multilayer ZnO thin films have a uniform surface composition. This is believed to be a result of the final annealing step. Lin et al. (24) reported a similar annealing temperature dependence on the concentration of vacancy defects and electron transport in metal oxide semiconductors.

Contrary to the uniformity in the XPS spectra of the top surface of single or 20 QSL thin films of ZnO, the photoluminescence (PL) spectra in Fig. 4(c) shows the various radiative electronic sub-band transitions causing the deep level defect emission from the single- and multi-layer thin films. PL emission from ZnO films is typically due to the presence of intrinsic defects such as Zn or O vacancies and interstitials. The defects which are believed to be the source of the measured emission are noted in Fig. 4(c).(25) The defect consistency, noted from the surface sensitive XPS measurements, is therefore shown to be only applicable to the sample surface, and not throughout the internal structure of the thin films. This variation in defect type and concentration highlight the impact of heat treatments on the formation and number of intrinsic defects in semiconductor growth. Further work is ongoing to determine the relationship between the volumetric defect density and the crystal orientation of each bilayer in the QSL. The multi-layer QSL system, however, received a significantly larger amount of heat energy from the drying steps of the deposition process, where samples are dried at ~ 260 ^{o}C for 5 mins between each iterative spin-coating. These QSL structures show specific green luminescence, recently reported to arise from Zn lattice vacancies dominant in m-plane oriented ZnO. The orange luminescence is attributed to the sublayer of each bilayer in the QSL, which comprises a nanocrystalline granular structure that likely contains significant surface to volume ratio.

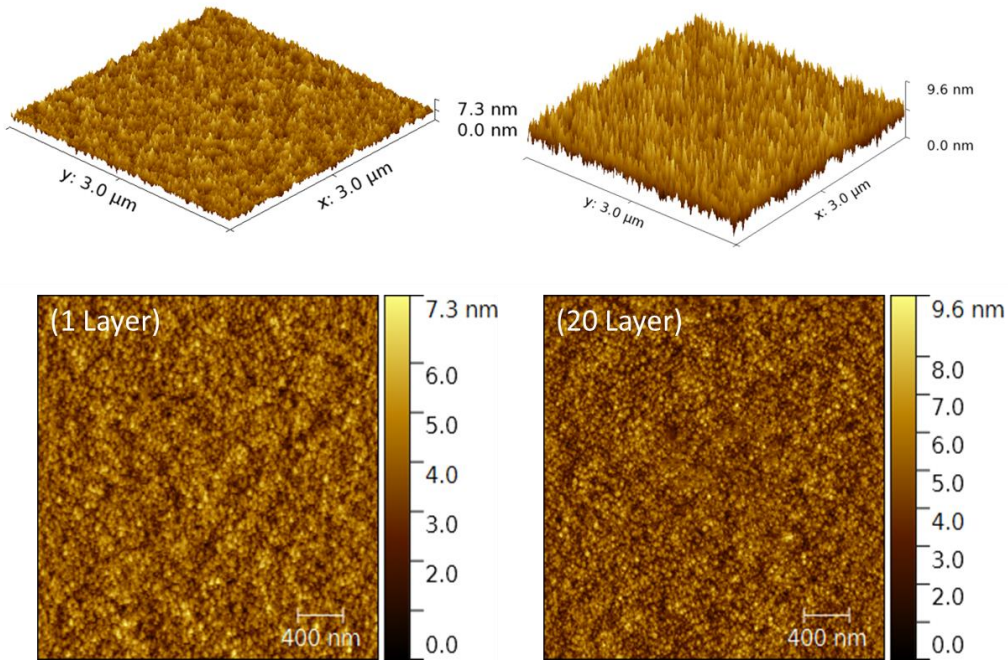

Figure 5. (Top) 3D AFM images showing the comparative roughness of 1 and 20 layer samples. (Bottom) AFM surface images for 1 and 20 layer ZnO thin films.

Atomic force microscopy (AFM) surface scans were taken of the 1 and 20 layer ZnO thin films in order to determine the surface morphology and roughness. Surface roughness is a key characteristic in developing TFT channel materials as it plays a crucial role in contact resistance. Figure 5 shows the 2D and the corresponding 3D representations of the single- and multi-layer topography, post-annealing. These surfaces show no obvious defects over an area of 3 μm × 3 μm. The absence of large grain boundaries in the films is also important to note for viability as an electronic material.

Table 1. RMS roughness values for 1 and 20 layer ZnO thin films.

Number of deposited layers	RMS Roughness (nm)
1	0.078
20	0.135

The root mean square (rms) roughness of the films, shown in Table 1, confirm that smooth and uniform thin films can be deposited from liquid precursors using a spin-coating method. During QSL film fabrication, deposition of precursor material for each grown layer occurs on the smooth upper surface of the previous ZnO film (denser capping layers as seen in Fig. 2) created during iterative drying stages. This allows the film to maintain a smooth and uniform top surface instead of becoming continuously rougher. Low rms roughness and the absence of large defects and grain boundaries highlight the morphological applicability of these spin-coated thin films as semiconductor channel materials in TFT devices.

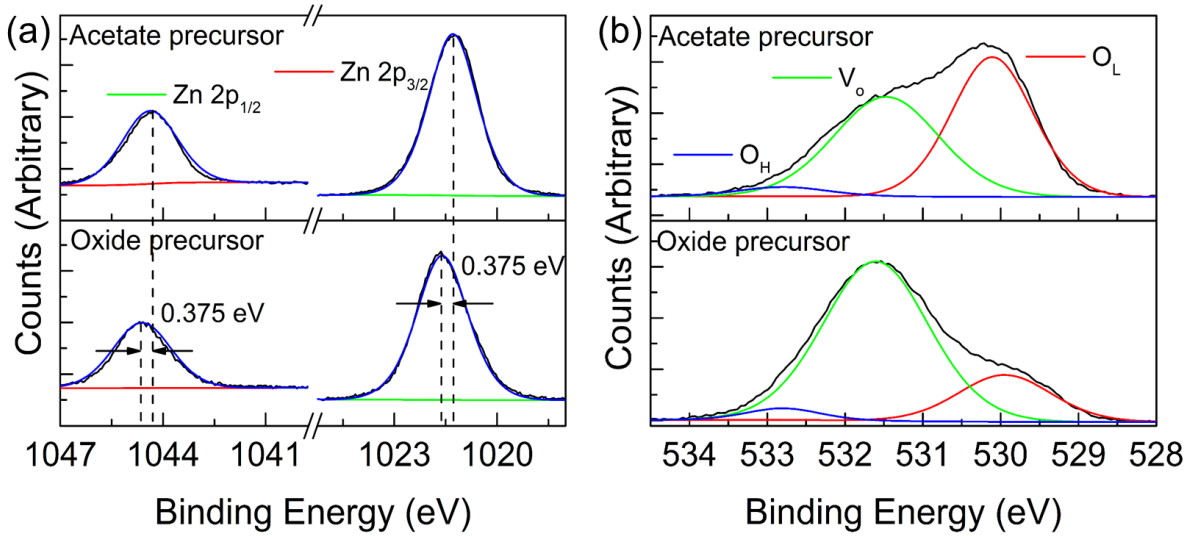

Figure 6. (a) Zn 2p core level XPS spectra and (b) O 1s core level spectra of ZnO thin films deposited from acetate and oxide precursors.

We also investigated the nature of the starting precursor on the compositional and electronic quality of the ZnO thin film. Figure 6 shows the Zn 2p and O 1s XPS spectra of thin films made from zinc acetate and zinc oxide precursors. The Zn 2p core level spectra, in Fig. 6(a), show a measured shift of 0.375 eV in the Zn 2p doublet to higher binding energies for samples made from the oxide precursor compared to those from acetate-based precursors under identical conditions. This shift is characteristic of an increase in the carrier density of the n-type conduction for the films made from the oxide precursor.

Samples made from the precursor of ZnO solubilized in ammonium hydroxide show relatively higher V_O concentrations than thin films from zinc acetate films, shown in Fig. 6(b). This is believed to be due to the abundance of oxygen present during the formation of the film. The precursor solution is comprised of pure ZnO dissolved in NH_4OH and subsequently annealed in air. This is thought to provide more than a sufficient amount of O^{2-} ions to bond to the Zn^{2+} ions in the lattice and leave remaining oxygen ions in the structure at oxygen vacant sites. With both precursor solutions the zinc ions would be the limiting factor for how much oxygen is found in the lattice, O_L, and any additional oxygen from the precursor or from annealing in air is found in the films at the oxygen vacancies. The levels of excess oxygen atoms were thought to be higher in the oxygen-rich zinc oxide precursors and therefore have larger V_O peaks. This higher O vacancy is representative of increased n-type characteristics in channel materials due to their nature as charge carrier donors, but also an ionized impurity scatterers. Further work is underway to determine the relationship between the composition, V_O content and n-type conductivity.

Conclusions

We detailed the growth of crystalline ZnO thin films and quasi superlattices on amorphous substrates with a periodic layered structure from a solution-based precursor via a spin-coating technique. ZnO films are grown from zinc acetate and zinc oxide-based precursors using the same approach. Electron microscopy and X-ray diffraction showed a periodic, epitaxial-like growth for multilayered films with a highly-ordered crystalline growth direction. Surface defect composition and concentration are shown to be consistent regardless of single-layer or QSL formation, with a higher number of deposited layers only affecting the internal electronic defects as measured by photoluminescence. Atomic force microscopy displayed a low-roughness, defect-free surface with no large grain boundaries. The effect of precursor material on the surface defects and electronic properties showed that an excess of oxygen before annealing in an open atmosphere leads to n-type characteristics. Spin-coating of thin films on amorphous substrates is shown to produce materials which are morphologically, compositionally and structurally suited to use as channel materials in TFT devices.

Acknowledgements

D.B. acknowledges the support of the Irish Research Council under award GOIPG/2014/206. COD acknowledges support from Science Foundation Ireland (SFI) through the SFI Technology Innovation and Development Award 2015 under contract 15/TIDA/2893 and by a research grant from SFI under grant Number 14/IA/2581.

References

1. K. Nomura, H. Ohta, A. Takagi, T. Kamiya, M. Hirano and H. Hosono, *Nature*, **432**, 488 (2004).
2. T. Kamiya, K. Nomura and H. Hosono, *Sci. Tech. Adv. Mater*, **11**, 044305 (2010).
3. R. A. Street, *Adv. Mater.*, **21**, 2007 (2009).
4. S. Shigehiko, H. Takeo, K. Motoki, K. Kazuto, Y. Mitsuaki and I. Masataka, *Jpn. J. Appl. Phys*, **47**, 2845 (2008).
5. J. Socratous, K. K. Banger, Y. Vaynzof, A. Sadhanala, A. D. Brown, A. Sepe, U. Steiner and H. Sirringhaus, *Adv. Funct. Mater.*, **25**, 1873 (2015).

6. H. Lingling, H. Dedong, C. Zhuofa, C. Yingying, W. Jing, Z. Nannan, D. Junchen, Z. Feilong, L. Lifeng, Z. Shengdong, Z. Xing and W. Yi, *Jpn. J. Appl. Phys*, **54**, 04DJ07 (2015).
7. M. Lorenz, M. S. R. Rao, T. Venkatesan, E. Fortunato, P. Barquinha, R. Branquinho, D. Salgueiro, R. Martins, E. Carlos, A. Liu, F. K. Shan, M. Grundmann, H. Boschker, J. Mukherjee, M. Priyadarshini, N. DasGupta, D. J. Rogers, F. H. Teherani, E. V. Sandana, P. Bove, K. Rietwyk, A. Zaban, A. Veziridis, A. Weidenkaff, M. Muralidhar, M. Murakami, S. Abel, J. Fompeyrine, J. Zuniga-Perez, R. Ramesh, N. A. Spaldin, S. Ostanin, V. Borisov, I. Mertig, V. Lazenka, G. Srinivasan, W. Prellier, M. Uchida, M. Kawasaki, R. Pentcheva, P. Gegenwart, F. M. Granozio, J. Fontcuberta and N. Pryds, *J. Phys. D: Appl. Phys.*, **49**, 433001 (2016).
8. Ü. Özgür, Y. I. Alivov, C. Liu, A. Teke, M. A. Reshchikov, S. Doğan, V. Avrutin, S.-J. Cho and H. Morkoç, *J. Appl. Phys.*, **98**, 041301 (2005).
9. E. Fortunato, P. Barquinha, A. Pimentel, A. Gonçalves, A. Marques, L. Pereira and R. Martins, *Thin Solid Films*, **487**, 205 (2005).
10. A. Lyubchyk, A. Vicente, P. U. Alves, B. Catela, B. Soule, T. Mateus, M. J. Mendes, H. Águas, E. Fortunato and R. Martins, *Phys. Status Solidi A*, **213**, 2317 (2016).
11. R. Martins, P. Barquinha, A. Pimentel, L. Pereira and E. Fortunato, *Phys. Status Solidi A*, **202**, R95 (2005).
12. P. Nunes, E. Fortunato, P. Tonello, F. Braz Fernandes, P. Vilarinho and R. Martins, *Vacuum*, **64**, 281 (2002).
13. E. M. C. Fortunato, P. M. C. Barquinha, A. C. M. B. G. Pimentel, A. M. F. Gonçalves, A. J. S. Marques, L. M. N. Pereira and R. F. P. Martins, *Adv. Mater.*, **17**, 590 (2005).
14. C. Glynn and C. O'Dwyer, *Adv. Mater. Interfaces.*, **4**, 1600610 (2016).
15. R. M. Pasquarelli, D. S. Ginley and R. O'Hayre, *Chem. Soc. Rev.*, **40**, 5406 (2011).
16. X. Yu, T. J. Marks and A. Facchetti, *Nat. Mater.*, **15**, 383 (2016).
17. C. Glynn, H. Geaney, D. McNulty, J. O'Connell, J. Holmes and C. O'Dwyer, *J. Vac. Sci. Technol. A*, **35**, 020602 (2017).
18. K. Si Joon, Y. Seokhyun and K. Hyun Jae, *Jpn. J. Appl. Phys.* **53**, 02BA02 (2014).
19. D. Buckley, R. McCormack, and C. O'Dwyer, *J. Phys. D: Appl. Phys.* doi: 10.1088/1361-6463/aa6559 (2017).
20. L. Liu, Z. Mei, A. Tang, A. Azarov, A. Kuznetsov, Q.-K. Xue and X. Du, *Phys. Rev. B: Condens. Matter*, **93**, 235305 (2016).
21. H.-B. Fan, S.-Y. Yang, P.-F. Zhang, H.-Y. Wei, X.-L. Liu, C.-M. Jiao, Q.-S. Zhu, Y.-H. Chen and Z.-G. Wang, *Chin. Phys. Lett* **24**, 2108 (2007).
22. M. N. Islam, T. B. Ghosh, K. L. Chopra and H. N. Acharya, *Thin Solid Films*, **280**, 20 (1996).
23. Y. Tak, D. Park and K. Yong, *J. Vac. Sci. Technol. B*, **24**, 2047 (2006).
24. Y.-H. Lin, S. R. Thomas, H. Faber, R. Li, M. A. McLachlan, P. A. Patsalas and T. D. Anthopoulos, *Adv. Electron. Mater.*, **2**, 1600070 (2016).
25. K. H. Tam, C. K. Cheung, Y. H. Leung, A. B. Djurišić, C. C. Ling, C. D. Beling, S. Fung, W. M. Kwok, W. K. Chan, D. L. Phillips, L. Ding and W. K. Ge, *J. Phys. Chem. B.*, **110**, 20865 (2006).